An Analytical 3D Laplacian Regularized SHORE Basis and Its Impact on EAP Reconstruction and Microstructure Recovery

Rutger Fick, Demian Wassermann, Gonzalo Sanguinetti, and Rachid Deriche

Abstract In diffusion MRI, the reconstructed Ensemble Average Propagator (EAP) from the diffusion signal provides detailed insights on the diffusion process and the underlying tissue microstructure. Recently, the Simple Harmonic Oscillator based Reconstruction and Estimation (SHORE) basis was proposed as a promising method to reconstruct the EAP. However, the fitting of the basis is sensitive to noise. To solve this we propose to use the Laplacian of the SHORE basis as a natural regularization functional. We provide the derivation of the Laplacian functional and compare its effect on EAP reconstruction with that of separated regularization of the radial and angular parts of the SHORE basis. To find optimal regularization weighting we use generalized cross-validation and validate our method quantitatively on synthetic and qualitatively on human data from the Human Connectome Project. We show that Laplacian regularization provides more accurate estimation of the signal and EAP based microstructural measures.

1 Introduction

In diffusion MRI, the acquisition and reconstruction of the diffusion signal in 3D **q**-space allows for the reconstruction of the water displacement probability, known as the Ensemble Average Propagator (EAP) [6, 16]. This EAP describes the probability density that a particle will move along a certain direction in a given diffusion time Δ. The EAP, or $P(\mathbf{r})$, is related to the diffusion signal by a Fourier transform.

$$P(\mathbf{r}) = \int_{\mathbb{R}^3} E(\mathbf{q}) e^{-2i\pi \mathbf{q}\cdot\mathbf{r}} d\mathbf{q} \tag{1}$$

where $\mathbf{r}$ is a displacement vector in $\mathbf{r}$-space and $E(\mathbf{q})$ is the measured diffusion signal at wave vector $\mathbf{q}$ sampled in $\mathbf{q}$-space. Here $\mathbf{q}$ is related to the applied magnetic field gradient magnitude, direction and duration [6, 16]. Historically, the diffusion

R. Fick (✉) • D. Wassermann • G. Sanguinetti • R. Deriche
Athena, Inria Sophia Antipolis – Méditerranée, France
e-mail: rutger.fick@inria.fr; demian.wassermann@inria.fr; gsangui@gmail.com; rachid.deriche@inria.fr

L. O'Donnell et al. (eds.), *Computational Diffusion MRI*, Mathematics and Visualization, DOI 10.1007/978-3-319-11182-7_14

tensor (DT) [4] was the first model to describe the EAP by assuming it lies within the family of Gaussian distributions, though this assumption also limits its ability to describe complex tissue structures. To overcome this limition, so-called high angular resolution diffusion imaging (HARDI) methods such as Q-ball imaging [18] and constrained spherical deconvolution [17] were developed that are able to resolve the directionality of more complicated fiber bundle configurations. However, these models still make restricting assumptions on the shape of the EAP, which limits their ability to describe the full 3D EAP in an unbiased way. It is possible to reconstruct the EAP without any prior knowledge or restrictions using acquisition schemes such as Diffusion Spectrum Imaging (DSI) [20]. Though, DSI's need for a numerical inverse Fourier transform of $E(\mathbf{q})$, which requires a dense and lengthy sampling of $\mathbf{q}$-space, limits its clinical applicability. Indeed, an important research topic has been the accurate reconstruction of the EAP with a reduced number of samples. As a solution, models that involve analytical representations of the signal have been proposed as they provide compact representation of the 3D $\mathbf{q}$-space signal and are less sensitive to noise. Such models include the Spherical Polar Fourier (SPF) basis [2], the Solid Harmonic (SoH) basis [10] and the Simple Harmonic Oscillator based Reconstruction and Estimation (SHORE) basis [12]. These bases capture the radial and angular properties of the diffusion signal by fitting a linear combination of orthogonal dual basis functions. With a dual basis, the coefficients describing the contribution of every basis function to the signal can also be used to describe the EAP. In this way $E(\mathbf{q})$ and $P(\mathbf{r})$ are represented as

$$E(\mathbf{q}) = \sum_{n=0}^{\infty} c_n \Xi_n(\mathbf{q}) \qquad P(\mathbf{r}) = \sum_{n=0}^{\infty} c_n \Upsilon_n(\mathbf{r}) \tag{2}$$

where coefficients c_n describe the contribution of dual basis functions Ξ_n to the signal and Υ_n to the EAP. However, the fitting of the basis is sensitive to noise and appropriate regularization is required. In literature several regularization methods have been developed for such bases, most of which try to enforce smoothness in the reconstructed signal. For example, in the SoH basis only an angular Laplace Beltrami regularization term was used [10]. For the SPF basis, the combination of a radial low-pass filter and an angular Laplace Beltrami regularizer was proposed [2] (which we will now call separated regularization). Later, it was shown that the Laplacian functional for the SPF basis outperformed separated regularization [7]. For the SHORE basis, a regularization using the Laplacian functional was proposed only for 1D-SHORE [14], while for 3D-SHORE separated regularization [11] and later quadratic programming [15] was used. As for a choice of basis, an advantage of SHORE over the others is that its elements are eigenvectors of the Fourier transform, a property that ensures rapid convergence in both real and Fourier spaces [19]. For this reason, in this work we focus on regularization for the SHORE basis. Inspired by what was proposed in [7] for the SPF basis, we propose to use the full 3D Laplacian regularization of the SHORE basis as it is well suited for the smooth nature of the diffusion signal. We validate our approach in three steps: First we

simulate the intra-axonal signal for a single white matter (WM) bundle and quantify signal reconstruction based on the estimation of microstructural measures known as the Return-To-Axis and Return-To-Origin probability (RTAP and RTOP). Secondly, we generate fiber crossings and compare signal and EAP reconstruction with respect to similarity to the ground truth, and finally we compare EAP projections and ODF visualizations on human data from the Human Connectome Project.

2 Theory

The SHORE basis [12, 15] was designed to reconstruct the diffusion signal and the EAP in the complete 3D space. In this basis the diffusion signal is given by

$$\Xi_{jlm}(u_0, \mathbf{q}) = \sqrt{4\pi} i^{-l} (2\pi^2 u_0^2 q^2)^{l/2} e^{-2\pi^2 u_0^2 q^2} L_{j-1}^{l+1/2}(4\pi^2 u_0^2 q^2) Y_l^m(\mathbf{u}_q) \quad (3)$$

where $j = (n + 2 - l)/2$ is related to the radial order n and angular order l where $j \geq 1, l \geq 0$ and $\mathbf{q} = q \cdot \mathbf{u}_q$ is the $\mathbf{q}$-space vector with q its magnitude and $\mathbf{u}_q$ its normalized orientation. The real spherical harmonic basis Y_l^m was introduced in [9] with angular order l and phase factor m such that $-l \leq m \leq l$. Here $L_{j-1}^{l+1/2}$ is the generalized Laguerre polynomial and u_0 is the isotropic scale factor related to the diffusivity of the measured data. The basis functions Υ_{jlm} of the EAP are obtained by the three-dimensional inverse Fourier transform of Ξ_{jlm} resulting in

$$\Upsilon_{jlm}(u_0, \mathbf{r}) = \frac{(-1)^{j-1}}{\sqrt{2}\pi u_0^3} \left(\frac{r^2}{2u_0^2}\right)^{l/2} e^{-r^2/2u_0^2} L_{j-1}^{l+1/2}\left(\frac{r^2}{u_0^2}\right) Y_l^m(\mathbf{u}_r) \quad (4)$$

where $\mathbf{r} = r \cdot \mathbf{u}_r$ is the r-space vector with r its magnitude and $\mathbf{u}_r$ its normalized orientation. When the propagator is assumed symmetric, as is a consequence of the acquisition protocol in diffusion MRI, the number of coefficients is given by $N_{\text{coef}} = 1/6(F + 1)(F + 2)(4F + 3)$ with $F = \lfloor n_{\max}/2 \rfloor$. Note that for both bases the angular dependence is only contained in the spherical harmonics function.

As the basis functions Ξ_{jlm} are orthonormal on $\mathbb{R}^3$, we use Eq. (2) to estimate the coefficients c_n from the entire $\mathbf{q}$-space data consisting of N_{data} points. The coefficients are cast into an N_{coef}-dimensional vector $\mathbf{c}$ and the signal values are placed in an N_{data}-dimensional vector $\mathbf{y}$. Design matrix $\mathbf{Q} \in \mathbb{R}^{N_{\text{data}} \times N_{\text{coef}}}$ then has elements $\mathbf{Q}_{ij} = \Xi_i(u_0, \mathbf{q}_j)$. With these definitions, Eq. (2) turns into the matrix equation $\mathbf{y} = \mathbf{Q}\mathbf{c}$. The coefficients $\mathbf{c}$ are found by solving the least squares problem $\mathbf{c} = \text{argmin}_{\mathbf{c}} \|\mathbf{y} - \mathbf{Q}\mathbf{c}\|^2 = (\mathbf{Q}^{\mathsf{T}}\mathbf{Q})^{-1}\mathbf{Q}^{\mathsf{T}}\mathbf{y}$. Note that $\mathbf{Q}$ needs to be recomputed for every voxel as u_0 is data dependent. The EAP can then be sampled at specific positions $\mathbf{r}$ using the matrix equation $\mathbf{r} = \mathbf{K}\mathbf{c}$, where matrix $\mathbf{K} \in \mathbb{R}^{N_{\text{sample}} \times N_{\text{coef}}}$ has elements $\mathbf{K}_{ij} = \Upsilon_i(u_0, \mathbf{r}_j)$ [15]. The basis fitting can then be regularized in different ways, which we explain in the next section.

2.1 Regularization

2.1.1 Laplacian Regularization

We propose to compute the Laplacian regularization term for the fitting procedure. In this case we want to minimize the quantity $\mathbf{c} = \text{argmin}_{\mathbf{c}} \|\mathbf{y} - \mathbf{Q}\mathbf{c}\|^2 + \lambda_\Delta U(\mathbf{c})$ where λ_Δ weights the regularization functional

$$U(\mathbf{c}) = \int_{\mathbb{R}^3} \|\Delta E_{\mathbf{c}}(\mathbf{q})\|^2 d\mathbf{q} \tag{5}$$

with $E_{\mathbf{c}}(\mathbf{q}) = \sum_i c_i \Xi_i(\mathbf{q})$ the reconstructed signal and Δ is the Laplacian operator. We can then express $E_{\mathbf{c}}(\mathbf{q})$ in a summation of SHORE basis functions

$$U(\mathbf{c}) = \int_{\mathbb{R}^3} \left(\sum_i c_i \Delta \Xi_i(\mathbf{q}) \right)^2 d\mathbf{q} = \sum_i \sum_k c_i c_k \int_{\mathbb{R}^3} \Delta \Xi_i(\mathbf{q}) \cdot \Delta \Xi_k(\mathbf{q})\, d\mathbf{q} \tag{6}$$

where the subscripts i and k indicate the radial and angular order of the ith or kth basis function $\Xi_i(\mathbf{q}) = \Xi_{j(i)l(i)m(i)}(\mathbf{q})$. We can write the summations in quadratic form such that $U(\mathbf{c}) = \mathbf{c}^\mathsf{T}\mathbf{R}\mathbf{c}$ where regularization matrix $\mathbf{R}$ has elements

$$\mathbf{R}_{ik} = \int_{\mathbb{R}^3} \Delta \Xi_i(\mathbf{q}) \cdot \Delta \Xi_k(\mathbf{q}) d\mathbf{q}. \tag{7}$$

The equation for the elements of $\mathbf{R}$ can be solved by using the general differential equation whose solutions form the functional basis functions Ξ_{jlm} of the SHORE basis

$$\left(-\frac{\Delta}{(2\pi u_0)^2} + (2\pi u_0)^2 q^2 \right) \Xi_{jlm}(\mathbf{q}) = \Lambda_{jlm} \Xi_{jlm}(\mathbf{q}) \tag{8}$$

with $\Lambda_{jlm} = 2l + 4j - 1$ [15]. By inverting this equation we can show that

$$\Delta \Xi_{jlm}(\mathbf{q}) = 4\pi^2 u_0^2 (4\pi^2 q^2 u_0^2 - \Lambda_{jlm}) \Xi_{jlm}(\mathbf{q}). \tag{9}$$

Inserting Eq. (9) into Eq. (7), using the fact that Y_l^m is an orthonormal basis with respect to the dot product on S^2 and $L_n^\alpha(x)$ is orthonormal with respect to the weighting function $x^\alpha e^{-x}$ on $[0, \infty)$, we find the general equation for $\mathbf{R}$ as

$$\mathbf{R}_{ik} = \delta_{(l(i),l(k))} \delta_{(m(i),m(k))} R\,(j(i), j(k), l) \tag{10}$$

where we define the intermediate function R as

$$R\left(j(i),j(k),l\right)=\begin{cases}\delta_{(j(i),j(k)+2)}\frac{2^{2-l}\pi^2u_0\Gamma\left(\frac{5}{2}+j(k)+l\right)}{\Gamma(j(k))}\\ \delta_{(j(i),j(k)+1)}\frac{2^{2-l}\pi^2u_0(-3+4j(i)+2l)\Gamma\left(\frac{3}{2}+j(k)+l\right)}{\Gamma(j(k))}\\ \delta_{(j(i),j(k))}\frac{2^{-l}\pi^2u_0\left(3+24j(i)^2+4(-2+l)l+12j(i)(-1+2l)\right)\Gamma\left(\frac{1}{2}+j(i)+l\right)}{\Gamma(j(i))}\\ \delta_{(j(i),j(k)-1)}\frac{2^{2-l}\pi^2u_0(-3+4j(k)+2l)\Gamma\left(\frac{3}{2}+j(i)+l\right)}{\Gamma(j(i))}\\ \delta_{(j(i),j(k)-2)}\frac{2^{2-l}\pi^2u_0\Gamma\left(\frac{5}{2}+j(i)+l\right)}{\Gamma(j(i))}\end{cases}\tag{11}$$

with δ the Dirac delta function. Note that regularization matrix $\mathbf{R}$ is symmetric, mostly sparse and its elements depend only on the ordering of the basis functions and their radial and angular indices j, l and m. Using this formulation we can compute $\mathbf{R}$ up to a given $n_{\max}$ and obtain the SHORE coefficients using penalized least squares with unique minimum

$$\mathbf{c}=(\mathbf{Q}^{\mathsf{T}}\mathbf{Q}+\lambda_{\Delta}\mathbf{R})^{-1}\mathbf{Q}^{\mathsf{T}}\mathbf{y}.\tag{12}$$

2.1.2 Separated Regularization

In [2] a regularization method was proposed involving a separated angular Laplace Beltrami functional $\mathbf{L}$ and a radial low pass filter $\mathbf{N}$. In this case the penalized least squares equation has unique minimum

$$\mathbf{c}=(\mathbf{Q}^{\mathsf{T}}\mathbf{Q}+\lambda_n\mathbf{N}^{\mathsf{T}}\mathbf{N}+\lambda_l\mathbf{L}^{\mathsf{T}}\mathbf{L})^{-1}\mathbf{Q}^{\mathsf{T}}\mathbf{y}\tag{13}$$

with regularization weights λ_n and λ_l. Note that separated regularization has two weighting parameters, whereas our Laplacian regularization only has one, making our approach easier to tune. In the next section we explain the methods to quantify the reconstruction quality of the signal and EAP.

3 Materials and Methods

To quantify the reconstruction quality of the signal and EAP we simulate two types of data. First we generate the restricted intra-axonal diffusion signal of a single white matter (WM) bundle. On this data we quantify reconstruction quality based on the similarity to the ground truth signal and EAP and on the estimation of a microstructural measure known as the Return-to-Axis Probability (RTAP). Secondly we compute fiber crossings using a multiple compartments Gaussian model on which we quantify signal and EAP reconstruction quality.

3.1 Microstructural Data Generation and Quantification

We first generate synthetic data using a recently introduced analytical model for intra-axonal diffusion [21]. Assuming axon diameters are Gamma-distributed, this model describes the restricted intra-axonal signal perpendicular to a WM bundle as

$$E_{\text{perp}}(q_\perp;\alpha,\beta) = {}_3F_2\left(\frac{3}{2},\frac{\alpha}{2}+1,\frac{\alpha}{2}+\frac{3}{2};2,3;-16\pi^2\beta^2q_\perp^2\right) \tag{14}$$

where ${}_3F_2$ is a generalized hypergeometric function, α and β are the shape and scale parameters of the Gamma distribution and $q_\perp$ is the norm of $\mathbf{q}$ perpendicular to the fiber path. We assume axial symmetry of the diffusion signal and free diffusion along the fiber path, i.e. $E_{\text{par}}(q_\parallel, D) = \exp(-4\pi^2 q_\parallel^2 D_\parallel)$ with $q_\parallel$ the parallel component of $\mathbf{q}$ and $D_\parallel$ the parallel free water diffusivity. We simulate the intra-axonal signal similar as in [3] to be

$$E_{\text{intra}}(\mathbf{q}) = E_{\text{perp}}(q_\perp;\alpha,\beta)E_{\text{par}}(q_\parallel, D_\parallel). \tag{15}$$

Using this model the restricted intra-axonal diffusion signal in the whole $\mathbf{q}$-space can be readily obtained for any Gamma distributed axon diameter distribution. Rician noise is then added with noise variance σ such that SNR $= 1/\sigma$.

To quantify signal reconstruction based on the microstructure we use two measures known as the Return-To-Axis and Return-To-Origin probability (RTAP and RTOP) [15]. These values are known to be sensitive to the anisotropy of WM tissue. RTAP is computed as the integral of the diffusion signal on the plane perpendicular to the fiber direction and RTOP is integral of the whole 3D diffusion signal.

$$RTAP = \int_{\mathbb{R}^2} E(\mathbf{q}_\perp)d\mathbf{q}_\perp \qquad RTOP = \int_{\mathbb{R}^3} E(\mathbf{q})d\mathbf{q} \tag{16}$$

Moreover, in the case of restricted intra-axonal diffusion in a single fiber path RTAP is related to the reciprocal of the mean cross-sectional area of the axons, i.e. $\langle A\rangle = 1/RTAP$ [13].

The computations of RTOP and RTAP rely on integrals of the complete q-space, which depend highly on the extrapolation of the signal beyond the $\mathbf{q}$-space truncation. To quantify the accuracy of the extrapolation we simulate the intra-axonal signal on three equispaced shells in $\mathbf{q}$-space with 90 samples each for 22 realistic axon diameter distributions [1]. We consider two scenarios: (1) varying the maximum q-value $q_{\max}$ included in the measurements while keeping the signal-to-noise ratio (SNR) constant and (2) varying SNR while keeping $q_{\max}$ constant. In both cases we fit SHORE to the signal with different regularization methods with $n_{\max} = 6$. We quantify the accuracy of RTAP by estimating $\langle A\rangle$ and comparing the results with the ground truth $\langle A\rangle_{gt}$, which can be computed using the parameters of the Gamma distribution as $\langle A\rangle_{gt} = \alpha(\alpha+1)\beta^2$. For RTOP we directly compare the estimated values with the 3D integrals of Eq. (15).

3.2 Fiber Crossing Data Generation

To further quantify the quality of both signal and EAP reconstruction we generate synthetic fiber crossing data. The signal is simulated using a multi-compartment Gaussian model

$$E(\mathbf{q}) = \sum_{m=1}^{M} f_m \exp(-2\pi^2 \mathbf{q}^\mathsf{T} \mathbf{D}_m \mathbf{q}) \tag{17}$$

where M is the number of compartments, f_m is the relative compartment size with $\sum_{m=1}^{M} f_m = 1$ and $\mathbf{D}_m$ the corresponding diffusion tensor. We use acquisition parameters from the Human Connectome Project (HCP) where three shells with b-values $\in [1{,}000, 2{,}000, 3{,}000]\,\mathrm{s/mm^2}$ are sampled 90 times each with 5 b_0 samples per shell. A cross-section of the ground truth of the signal and EAP of an $M = 2, 72$ degree crossing with $f_1 = 0.6$ and $f_2 = 0.4$ is shown in Fig. 1. Again, Rician noise is added with noise variance σ such that SNR $= 1/\sigma$. Figure 2 shows the signal from Fig. 1a for three different noise levels. We then fit SHORE using separated and Laplacian regularization and compare signal and EAP reconstruction using the metrics given in the next section.

3.3 Error Metrics

We define two error metrics to quantify the reconstruction quality of the signal and EAP in the single WM bundle data and the multiple compartment Gaussian model. For the signal we use the L_2 metric

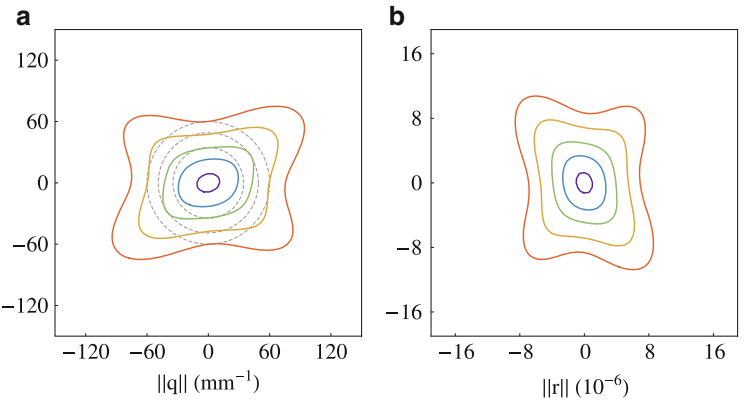

Fig. 1 Isocontour representations of the ground truth of the signal as a function of **q** (**a**) and the EAP as a function of **r** (**b**). The isocontours are color-labeled from *dark blue* (0.95 of maximum value) to *red* (0.1 of maximum value). The *dashed grey circles* in the signal represent the measured shells in **q**-space. (**a**) Ground truth signal. (**b**) Ground truth EAP

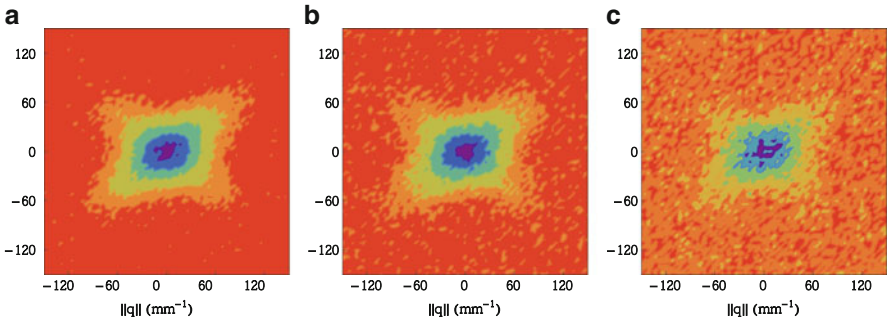

Fig. 2 The signal from Fig. 1a corrupted by Rician Noise. (**a**) SNR=30; (**b**) SNR=20; (**c**) SNR=10

$$\mathrm{L}_2(\mathbf{c}) = \int_{\mathbb{R}^3} (E_{\mathrm{GT}}(\mathbf{q}) - E_{\mathbf{c}}(\mathbf{q}))^2 d\mathbf{q} \tag{18}$$

where $E_{\mathrm{GT}}(\mathbf{q})$ is the ground truth signal and $E_{\mathbf{c}}(\mathbf{q})$ is the reconstructed signal with coefficients $\mathbf{c}$. For the EAP we use the Bhattacharyya distance (BD) [5] as it is a real metric between probability densities

$$\mathrm{BD}(\mathbf{c}) = -\ln\left(\int_{\mathbb{R}^3} \sqrt{P_{\mathrm{GT}}(\mathbf{r}) P_{\mathbf{c}}(\mathbf{r})} d\mathbf{r}\right) \tag{19}$$

where $P_{\mathrm{GT}}(\mathbf{r})$ and $P_{\mathbf{c}}(\mathbf{r})$ are the ground truth and reconstructed probability density functions of the EAP. We use these metrics to analyze the reconstruction quality for different regularization methods in the next section.

3.4 Optimal Weighting Parameter Choice

To fairly compare EAP reconstructions, we use the Generalized Cross Validation (GCV) algorithm [8] to obtain optimal regularization parameters λ_n, λ_l and λ_Δ. GCV is based on an N_{data}-fold cross validation. Fortunately, the estimation of λ as the minimum argument of the GCV function can be calculated as

$$GCV(\lambda, \mathbf{y}) = \frac{\|\mathbf{y} - \hat{\mathbf{y}}_\lambda\|}{N_{\mathrm{data}} - Tr(\mathbf{S}_\lambda)} \tag{20}$$

where $\mathbf{S}_\lambda = \mathbf{Q}(\mathbf{Q}^{\mathsf{T}}\mathbf{Q} + \lambda\mathbf{R})^{-1}\mathbf{Q}^{\mathsf{T}}$ is the smoother matrix and $\hat{\mathbf{y}}_\lambda = \mathbf{S}_\lambda\mathbf{y}$. Here $\mathbf{R}$ can contain multiple regularization functionals that can be optimized.

4 Results

4.1 Microstructure Experiments

To compare signal and EAP reconstruction quality on a single WM bundle between separated and Laplacian regularization we simulated the intra-axonal signal on three equispaced shells in **q**-space with 90 samples each for 22 realistic axon diameter distributions [1] as outlined in Eq. (14). We only generate the intra-axonal diffusion signal for two scenarios: in the first we vary $q_{\max}$ from 10 to 310 mm^{-1} in steps of 30 mm^{-1} while keeping $SNR = 20$. In the second we vary SNR between noiseless and $SNR = 5$ while keeping $q_{\max}$ at 200 mm^{-1}. In both cases we regenerate the noise 100 times per $q_{\max}$ or SNR and average the results over all axon diameter distributions and noise generations. For both datasets we compute the averaged absolute error between the estimated mean cross-sectional area $\langle A \rangle$ and ground truth $\langle A \rangle_{\mathrm{gt}}$ (Fig. 5b and c) and the values for RTOP with the ground truth (Fig. 5d and e). We do not show the results for the least squares solution as the extrapolation of the signal without regularization is completely unreliable (see Fig. 5a). It should be noted that using separated regularization approximately 2–3 % of all RTAP and RTOP estimates yield negative values, while this is only 0.03 % for Laplacian regularization.

4.2 Fiber Crossing Experiment

To quantify general fitting of the signal and EAP, the SHORE basis was fitted on a 72 degree crossing using separated and Laplacian regularization. In Fig. 3 we show the average L_2 and BD metrics for the reconstruction of the signal and EAP for 300 repetitions for every SNR. It is seen that Laplacian regularization has the lowest metrics and standard deviation for both the signal and the EAP. Furthermore, in Table 1 we show the variances for the weighting parameters,

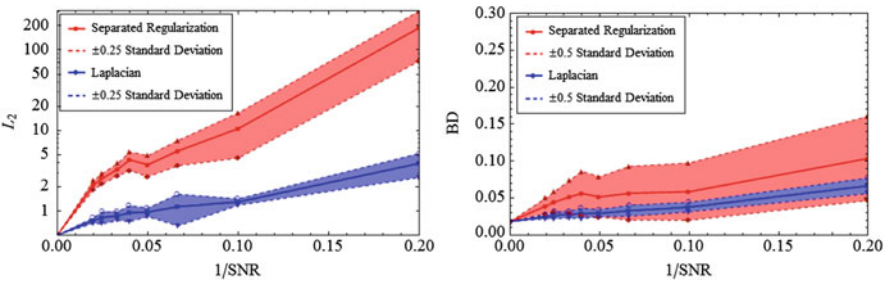

Fig. 3 The error metrics for the reconstruction of (*left*) the signal (L_2) and (*right*) the EAP (DB) as a function of 1/SNR. The L_2 plot for the signal is on a logarithmic scale. It can be seen that the Laplacian better and more reliably approximates the signal and EAP for all SNR

Table 1 Weighting parameter variances as a function of SNR

	1/SNR	0	0.02	0.025	0.033	0.040	0.050	0.067	0.100	0.200
Separated	Var(λ_n)	0	0.033	0.015	0.043	0.058	0.116	0.078	0.107	0.135
	Var(λ_l)	0	0.040	0.050	0.078	0.073	0.089	0.081	0.035	0.17
	Corr(λ_n,λ_l)	0	−0.461	−0.456	−0.633	−0.728	−0.797	−0.785	−0.727	−0.708
Laplacian	Var(λ_Δ)	0	0.027	0.028	0.030	0.026	0.026	0.031	0.057	0.031

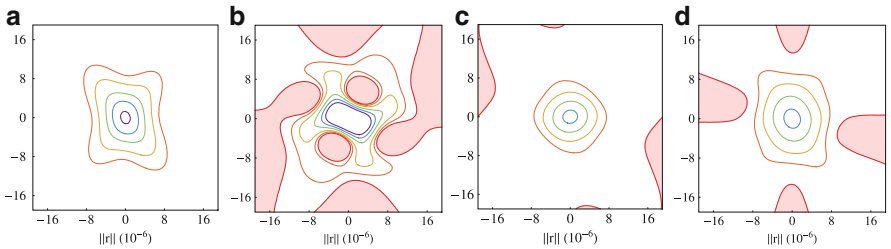

Fig. 4 A section of the ground truth of the EAP (**a**) with EAP reconstructions using no (**b**), separated (**c**) and Laplacian regularization (**d**). Noise was added such that $1/SNR = 0.1$. The *red* areas indicate negative values. The Laplacian best preserves the angular shape of the ground truth among the given methods. (**a**) EAP GT; (**b**) EAP LS; (**c**) EAP Sep; (**d**) EAP Lap

together with the Pearson correlation between λ_n and λ_l for every SNR. It can be seen that the variance for the Laplacian is much lower than those of the separated regularization. Finally, to give a visual interpretation to the graphs in Fig. 3 we show EAP reconstructions with different regularization methods at $1/SNR = 0.1$ together with the ground truth in Fig. 4. It can be seen that Laplacian regularization maintains the best angular characteristics of the ground truth, given that the signal is severely distorted (see Fig. 2c).

4.3 Human Connectome Project

In our last experiment we use the Human Connectome Project data, which was sampled on three shells with b-values $\in [1{,}000, 2{,}000, 3{,}000]\,\mathrm{s/mm^2}$, with 90 directions per shell. We selected a section in the brain near the Corpus Callosum (see Fig 6). In order to highlight reconstruction differences in the case of more noisy images we add noise to the data such that SNR = 20. We used GCV to obtain optimal weighting parameters for every voxel and we fit SHORE using $n_{\max} = 6$. In Fig. 6 we visualize the EAP at a radius of 10 and 20 μm and the ODFs using separated and our Laplacian regularization. The spherical representation of the EAP $P(\mathbf{r})$ at a certain radius $\mathbf{r}$ shows the relative probability of particles traveling this distance in the given diffusion time. It can be seen that the Laplacian attenuates spurious behaviour in the lower radius of the EAP (yellow box), though this effect is not as prominent in the ODF.

5 Discussion and Conclusion

In this paper we proposed and derived the full 3D Laplacian functional as a regularization for the fitting of the SHORE basis. We compared our proposed regularization with the previously proposed separated Laplace–Beltrami and radial low-pass filtering [2]. In our first experiment we show that Laplacian regularization

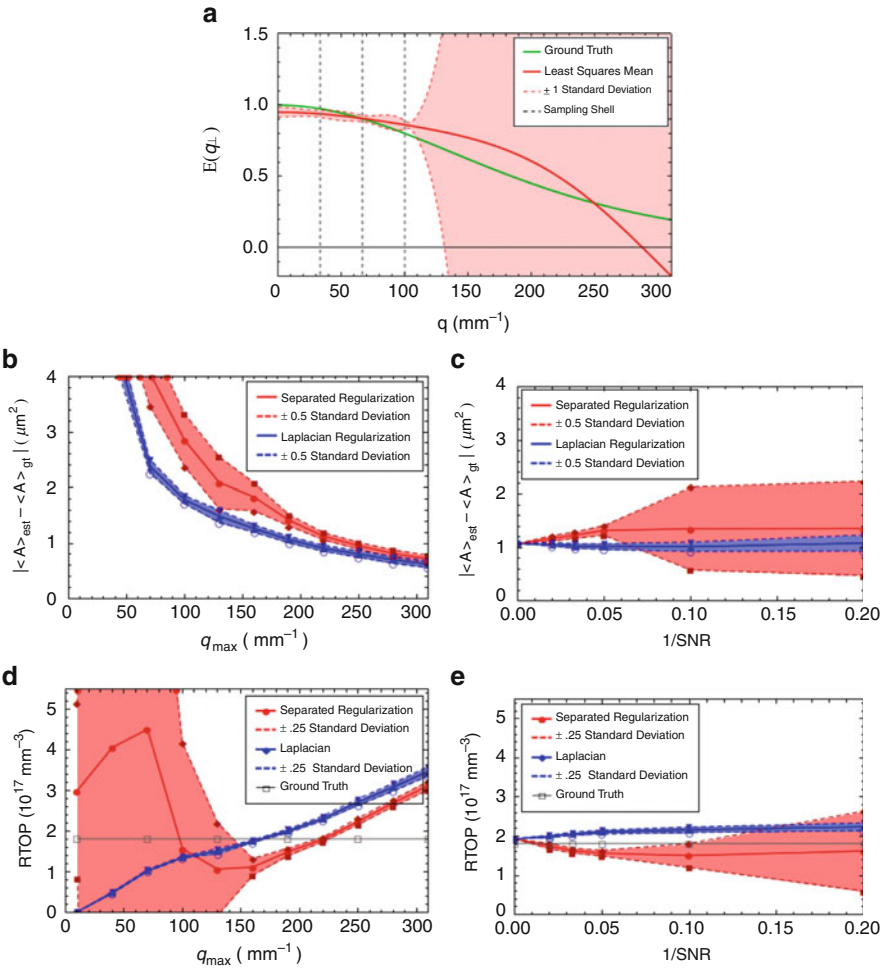

Fig. 5 (**a**) shows the Least Squares signal approximation. The *red area* indicates one standard deviation of the approximation. It can be seen that after the last sampling shell (the *grey dashed line*) the extrapolation is unreliable. (**b**) and (**c**) show the error in $\langle A \rangle$ for different regularization methods as a function of $q_{\max}$ and SNR. (**d**) and (**e**) show the values of RTOP with the ground truth. Both (**b**) and (**c**) show lower average error and lower standard deviations with Laplacian regularization under all $q_{\max}$ and SNR. (**d**) shows that with Laplacian regularization the estimated RTOP approaches the ground truth at $q_{\max}$ near 160 mm^{-1} but continues to grow as $q_{\max}$ increases. Moreover, it can be seen that RTOP for separated regularization has very unreliable estimates for low $q_{\max}$. Only after a $q_{\max}$ of 160 mm^{-1} the estimation stabilizes and a similar trend is seen of increasing RTOP as $q_{\max}$ increases. In (**e**) it can be seen that the mean RTOP becomes slightly higher than the ground truth for Laplacian regularization and slightly lower for separated regularization as SNR becomes lower. Again the Laplacian benefits from much lower standard deviations

of the SHORE basis provides more reliable estimates of microstructural features compared to separated regularization (Fig. 5). When comparing the mean and

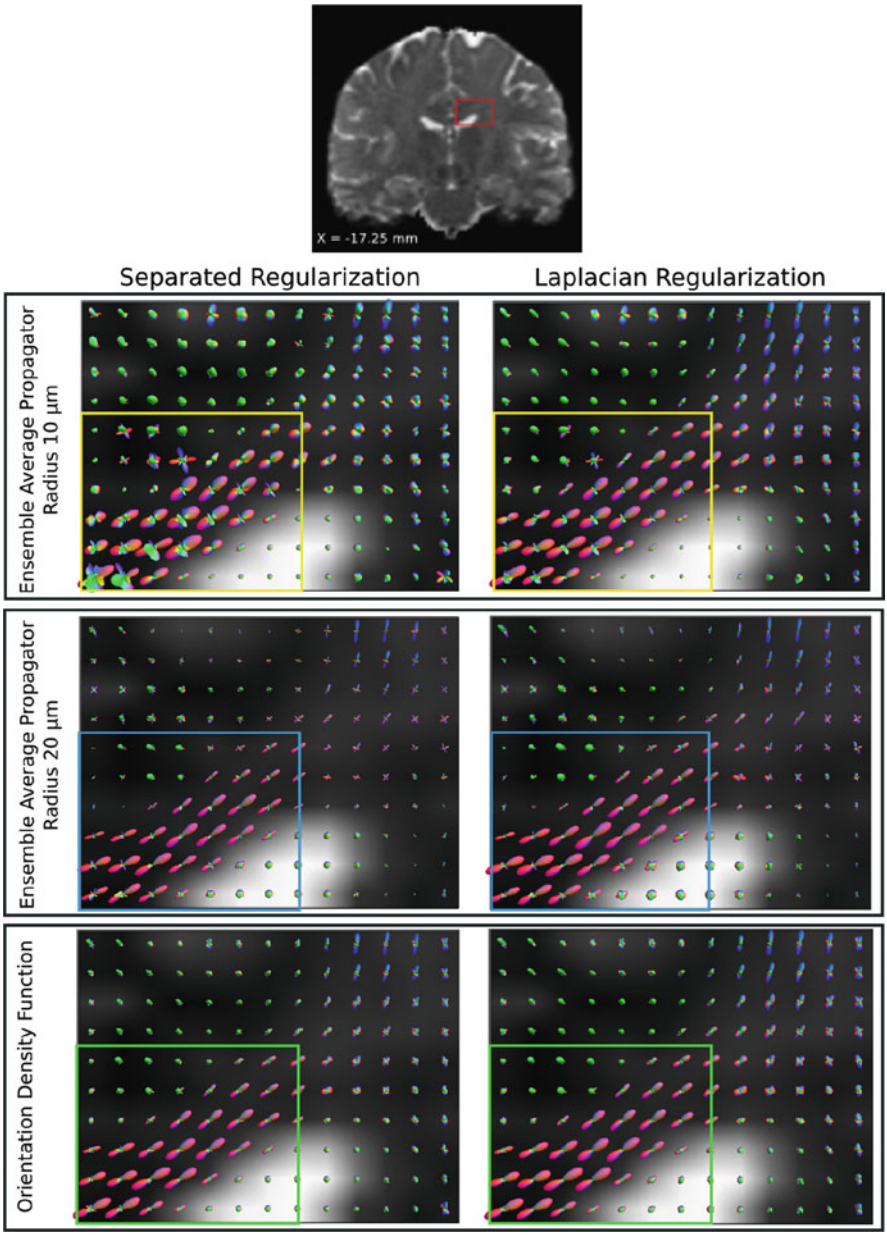

Fig. 6 Reconstructions of the EAP and ODF in an area near the Corpus Callosum of the Human Connectome Project using separated regularization (*left column*) and Laplacian regularization (*right column*). The EAP is reconstructed for two EAP radii (*top two rows*) and ODFs is given on the *bottom*. The Laplacian regularization stops spurious behaviour in the EAP compared to separated regularization (*yellow and blue rectangles*), though this effect is not as noticeable in the ODFs (*green rectangles*)

standard deviation of RTAP and RTOP between regularization methods, it can be seen that Laplacian regularization greatly improves signal extrapolation and robustness to noise at lower **q**-values and low SNR levels. The fact that almost no negative values for microstructural values were found using the Laplacian further underlines this result.

Moreover, in our second experiment we show that Laplacian regularization enables better and more reliable approximation of the signal and EAP in crossings (Fig. 3) and that the angular features of the EAP are better maintained under high levels of noise compared to separated regularization (Fig. 4). We also show that the estimation of the optimal weighting parameter is more stable for the Laplacian than for the separated implementation (Table 1), which suggests that our approach is better suited for this type of data. Finally, we provide visualization of the EAP and ODF on the Human Connectome Project dataset (Fig. 6). It can be seen that the influence of the regularization, while visible in the EAP, is not as noticeable on the ODFs.

Nonetheless, combined with the results of the other experiments in this work, we believe that the accurate approximation of the signal and EAP is essential to understanding the underlying microstructure, and appropriate regularization such as our Laplacian approach is therefore fundamental.

Acknowledgements Data were provided [in part] by the Human Connectome Project, WU-Minn Consortium (Principal Investigators: David Van Essen and Kamil Ugurbil; 1U54MH091657) funded by the 16 NIH Institutes and Centers that support the NIH Blueprint for Neuroscience Research; and by the McDonnell Center for Systems Neuroscience at Washington University.

References

1. Alexander, D.C.: A general framework for experiment design in diffusion MRI and its application in measuring direct tissue-microstructure features. Magn. Reson. Med. **60**, 439–448 (2008)
2. Assemlal, H.E., et al.: Efficient and Robust Computation of PDF features from diffusion MR signal. Med. Image. Anal. **13**(5), 715–729 (2009)
3. Avram, L., et al.: Three-dimensional water diffusion in impermeable cylindrical tubes: theory versus experiments. NMR Biomed. **21**(8), 888–898 (2008)
4. Basser, P.J., et al.: Estimation of the effective self-diffusion tensor from the NMR Spin Echo. J. Magn. Reson. Ser. B **103**(3), 247–254 (1994)
5. Bhattacharyya, A.: On a measure of divergence between two statistical populations defined by their probability distributions. Bull. Calcutta Math. Soc. **35**, 99–109 (1943)
6. Callaghan, P.T., et al.: High-resolution q-space imaging in porous structures. J. Magn. Reson. **90**(1), 177–182 (1990)
7. Caruyer, E., et al.: Diffusion MRI signal reconstruction with continuity constraint and optimal regularization. Med. Image. Anal. **16**(6), 1113–1120 (2012)
8. Craven, P., et al.: Smoothing noisy data with spline functions. Numer. Math. **31**(4), 377–403 (1978)
9. Descoteaux, M., et al.: Regularized, fast, and Robust analytical Q ball imaging. Magn. Reson. Med. **58**(3), 497–510 (2007)

10. Descoteaux, M., et al.: Multiple Q-shell diffusion propagator imaging. Med. Image. Anal. **15**(4), 603–621 (2011)
11. Merlet, S., et al.: Continuous diffusion signal, EAP and ODF estimation via compressive sensing in diffusion MRI. Med. Image. Anal. **17**(5), 556–572 (2013)
12. Özarslan, E., et al.: Simple harmonic oscillator based reconstruction and estimation for three-dimensional Q-space MRI (2009)
13. Özarslan, E., et al.: Nuclear magnetic resonance characterization of general compartment size distributions. New J. Phys. **13**(1), 015010 (2011)
14. Özarslan, E., et al.: Temporal scaling characteristics of diffusion as a new MRI contrast: findings in rat hippocampus. Neuroimage **60**(2), 1380–1393 (2012)
15. Özarslan, E., et al.: Mean apparent propagator (MAP) MRI: a novel diffusion imaging method for mapping tissue microstructure. NeuroImage **78**, 16–32 (2013)
16. Stejskal, E.O.: Use of spin echoes in a pulsed magnetic-field gradient study anisotropic restricted diffusion flow. J. Chem. Phys. **43**(10), 3597–3603 (1965)
17. Tournier, J., et al.: Robust determination of the fibre orientation distribution in diffusion MRI: non-negativity constrained super-resolved spherical deconvolution. NeuroImage **35**(4), 1459–1472 (2007)
18. Tuch, D.S.: Q-ball imaging. Magn. Reson. Med. **52**(6), 1358–1372 (2004)
19. Walter, G.G.: Properties of Hermite series estimation of probability density. Ann. Stat. **5**, 1258–1264 (1977)
20. Wedeen, V.J., et al.: Mapping complex tissue architecture with diffusion spectrum magnetic resonance imaging. Magn. Reson. Med. **54**(6), 1377–1386 (2005)
21. Sanguinetti, G., Deriche, R.: Mapping average axon diameters under long diffusion time. ISBI (2014)